AGU PUBLICATIONS

Geophysical Research Letters

RESEARCH LETTER
10.1002/2017GL073641

Key Points:
- A framework to predict the rheology of clay-rich suspensions in volcanic lakes
- Quantitative regime boundaries between viscous and brittle eruption behavior in clay suspensions
- Observations of steam-driven eruptions through lakes can be diagnostic of clay content

Supporting Information:
- Supporting Information S1
- Movie S1
- Movie S2

Correspondence to:
D. Schmid,
danamia23@gmail.com

Citation:
Schmid, D., B. Scheu, F. B. Wadsworth, B. M. Kennedy, A. Jolly, and D. B. Dingwell (2017), A viscous-to-brittle transition in eruptions through clay suspensions, *Geophys. Res. Lett.*, *44*, 4806–4813, doi:10.1002/2017GL073641.

Received 28 MAR 2017
Accepted 10 MAY 2017
Accepted article online 11 MAY 2017
Published online 27 MAY 2017

A viscous-to-brittle transition in eruptions through clay suspensions

Diana Schmid[1], Bettina Scheu[1], Fabian B. Wadsworth[1], Ben M. Kennedy[2], Arthur Jolly[3], and Donald B. Dingwell[1]

[1]Earth and Environmental Science, LMU Munich, Munich, Germany, [2]Geological Sciences, University of Canterbury, Christchurch, New Zealand, [3]GNS Science, Lower Hutt, New Zealand

Abstract Volcanic lakes are often associated with active geothermal circulation, mineral alteration, and precipitation, each of which can complicate the analysis of shallow magma physics, geophysical signals, and chemical signals. The rheology of the lake and associated hydrothermal system affects the eruptive activity as bubbles ascend and burst through the lake producing distinct ejection behavior. We investigate such phenomena by conducting scaled experiments in which heated water-clay suspensions are decompressed rapidly from relevant pressures. After a jet phase of expanding vapor, the suspensions break up into ejecta that are either angular or droplet geometry. We parameterize these regimes and find a universal clay volume fraction of 0.28 below which the ejecta are form droplets and above which the ejecta are angular. We propose a regime diagram for optical observations of active lakes, which allows rheological characterization and informs volcanic monitoring.

1. Introduction

Lakes in active volcanic environments are a common phenomenon exhibiting a variability in size, location relative to the vent, fluid composition, and lifetime. Volcanic and geothermal lakes and pools are often formed in craters of magmatic or phreatic eruptions, implying that they are perched over potentially active magmatic sources [*Fournier et al.*, 2009; *Christenson et al.*, 2015]. As such, exchange of mass between volcanic lakes and a hydrothermal system is commonplace, causing changes in temperature, acidity, and composition [*Oppenheimer*, 1997; *Varekamp*, 2015] and often favoring the formation of fine-grained suspensions of primary volcanic products, mineral precipitates, and alteration products. Further, it fosters strong lake water convection, overturn, and mixing of lake bottom sediments with lake water favoring the development of suspensions [*Christenson et al.*, 2015]. Mud pools are one manifestation of such activity and are found at various places within Taupo Volcanic Zone (New Zealand), Yellowstone and Lassen Volcanic National Park (USA), Beppu (Japan), Námafjall (Iceland), and Rincón de la Vieja Volcano National Park (Costa Rica), to name but a few examples. Similarly, volcanic lakes with fine-grained suspensions are the dominant lake fluid occurring at Poás (Costa Rica), Oyunama Lake (Hokkaido, Japan), Yu kun crater, Usu (Hokkaido, Japan), Boiling Lake (Dominica), Kawah Ijen (Indonesia), Lake Voui at Aoba volcano (Vanuatu), and Ruapehu and White Island (both New Zealand). Many of these lakes are repeatedly pierced by eruptions, which throw suspension material out of the lake in an explosion-driven eruption [*Christenson et al.*, 2010; *Fischer et al.*, 2015; *Jolly et al.*, 2016]. This kind of ejection of material from an explosive event occurring at the surface of a muddy lake represents a significant hazard that has not been well investigated such that surface observations are not yet diagnostic of eruption mechanisms or conditions.

Beginning in 2013, a hydrothermal eruption episode occurred at White Island (New Zealand), intersecting a shallow mud pool that varied in size and consistency over the course of the episode. White Island's eruptive activity was well documented over this entire episode, and four different eruption regimes have been identified [*Edwards et al.*, 2017]: (1) geometrically irregular and nonperiodic bursting on the lake surface, (2) larger regular or weakly periodic bursts that are preceded by hemispherical bulging of the lake surface and are followed by a mud heave and particulate ejection, (3) a vertical steam jet occasionally followed by a mud heave, and (4) lake draining and a period of dry lake conditions in which blocks are ejected from the lower vent. To date, this kind of observational detail is unique to this episode at White Island, but these behaviors are likely to be common to many muddy, clay-rich volcanic lakes.

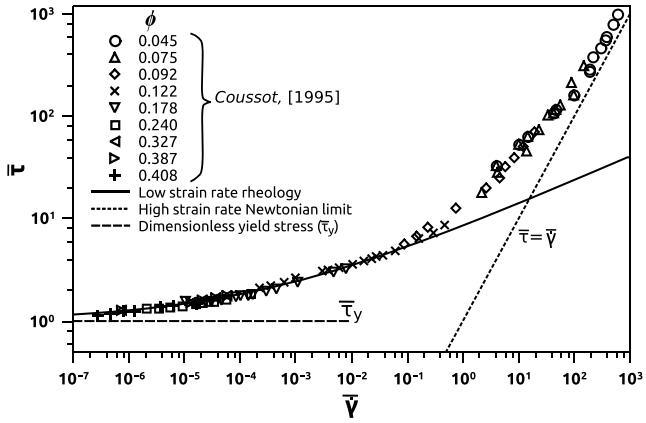

Figure 1. The rheology of a kaolin-water mixture here cast as the relationship between dimensionless shear stress $\bar{\tau}$ and dimensionless strain rate $\bar{\dot{\gamma}}$ for a range of ϕ. Both the data and the analysis are modified after *Coussot* [1995]. After *Coussot* [1995], we use a conceptual shift from a low- to high-strain rate rheology (see the text for details of the scaling used).

Here we present laboratory constraint of the parameters that likely drive muddy suspensions to eject in different regimes during eruptions under realistic pressure and temperature conditions. In doing so, we characterize the fundamental behavior of muddy suspensions, scaling our results to episodes such as the 2013 eruptive episode of White Island. We primarily explore the first-order effect of water content on the eruptive behavior, a variable which fluctuates significantly during eruptive sequences [*Edwards et al.*, 2017].

2. Materials, Fundamental Rheology, and Methods

The solid component of natural mud pool and volcanic lakes with significant suspensions can vary in grain size and composition, and it can comprise unaltered volcanic ash and nonmagmatic unconsolidated sediments as well as their alteration products—often various types of clays [*Christenson et al.*, 2015].

In the study presented here, we simplify this to a single component of constant grain size. We used a mixture of kaolin powder ($Al_4(OH)_8Si_4O_{10}$; Kremer Pigmente, GmbH & Co.) and water. The mass fraction of kaolin powder N was varied systematically between 0 and 0.58 (where the water mass fraction in this binary system is $1-N$). Mixtures with $N>0.58$ started to clump, form aggregates and incorporate air, and were therefore avoided. However, we also conducted experiments with $N=1$ to capture the behavior of pure solid as an end-member. The mixtures were colored with a Harold Scholz & Co. (GmbH) dye in order to achieve good contrast of the fluid against the condensing water vapor phase in high-speed videography of decompression tests (see below). As we only use two to three drops of dye, we consider the effect on the rheology to be negligible. We convert the mass fractions into volume fractions ϕ by $\phi=N(\Delta\rho)$, where $\Delta\rho$ is the ratio of the density of the total mixture to that of the clay particles (2600 kg m^{-3}).

As ϕ increases from $\phi=0$ (water), kaolin-water mixtures exhibit a non-Newtonian, shear-thinning relationship between shear stress and resultant shear strain rate and an increasing apparent yield stress [*Hulme*, 1974; *Huang and Garcia*, 1998; *Balmforth et al.*, 2000]. In Figure 1 we present literature data compiled from *Coussot* [1995] in which a variety of clay-in-water suspensions are characterized rheologically. After *Coussot* [1995], we demonstrate that when the data are rendered dimensionless, common behavior is seen across all clay contents. Two-dimensional groups are defined. First, a dimensionless shear stress $\bar{\tau}$ which is the ratio of the applied shear stress τ to a critical yield value τ_y such that $\bar{\tau}=\tau/\tau_y$ and the dimensionless yield stress $\bar{\tau}_y$ occurs at $\bar{\tau}=1$. Second, a dimensionless strain rate $\bar{\dot{\gamma}}$ which is a combination of τ_y, the strain rate $\dot{\gamma}$ and the viscosity of the suspension without shearing η, such that $\bar{\dot{\gamma}}=\eta\dot{\gamma}/\tau_y$. While τ and $\dot{\gamma}$ are measured values, we must choose a scaling for η and τ_y as a function of ϕ. We follow *Coussot* [1995] in choosing the empirical $\tau_y=a\exp(b\phi)$ with $a=0.1$ and $b=23$ for kaolin clay particles in water. We note that η could be taken to be any law for how suspended particle volume fraction affects the viscosity of a mixture, such as that of *Maron and Pierce* [1956]. However, for consistency, we use $\eta=\mu[1+0.75/(\phi_m/\phi-1)]^2$ [*Chong et al.*, 1971] as used by *Coussot* [1995], where μ is the viscosity of the Newtonian suspending liquid and ϕ_m is a maximum packing fraction of the clay particles beyond which the suspension is rigid. We use $\phi_m=0.7$, a maximum packing value consistent with nonspherical particles [*Mader et al.*, 2013]. When we plot $\bar{\tau}$ as a function of $\bar{\dot{\gamma}}$, we see a universal collapse of the rheological data to the desirable limits of $\bar{\tau}=\bar{\tau}_y=1$ at low $\bar{\dot{\gamma}}$ and to a Newtonian $\bar{\tau}=\bar{\dot{\gamma}}$ at high $\bar{\dot{\gamma}}$. *Coussot* [1995] propose a simple empirical low-$\bar{\dot{\gamma}}$ description as $\bar{\tau}=1+K\bar{\dot{\gamma}}^n$ with $K=7.6$ and $n=0.24$ for kaolin in water.

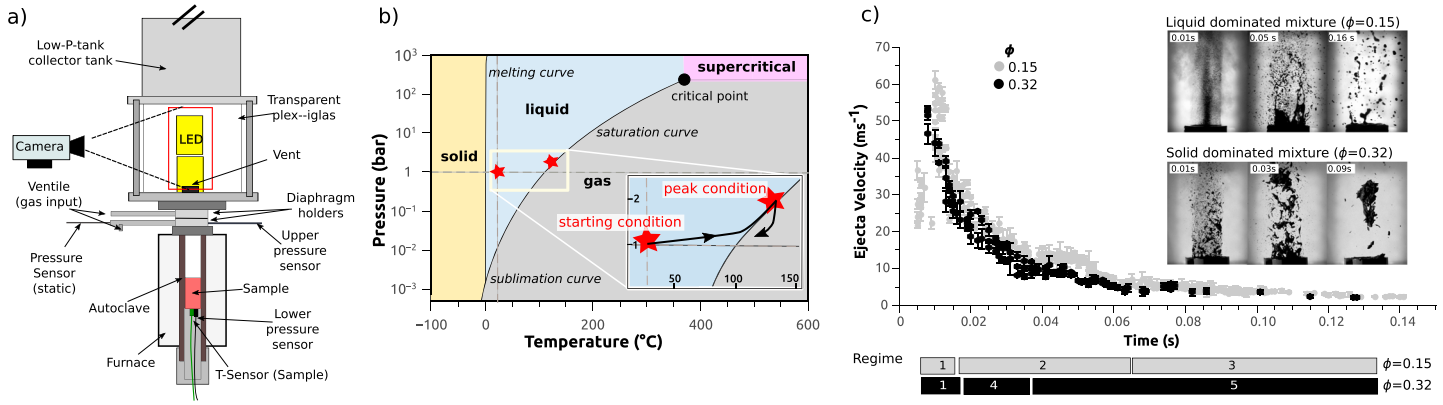

Figure 2. The experimental apparatus and conditions used to reproduce eruptions of clay-rich material. (a) Here we use an externally heated autoclave mounted below a decompression tank where we can record the ejection of the material using high-speed videography. The two sections (autoclave and tank) are separated by pressure resistant aluminum diaphragms that rupture at a known pressure 2 bar. We monitor continuously the sample temperature and the autoclave gas pressure. (b) A simplified phase diagram for water showing that as we heat the kaolin-water mixture at fixed volume to experimental conditions, the pressure increase is given by linear expansion and by the boiling curve. Decompression by diaphragm rupture then results in a large volume change and concomitant pressure drop, effectively vaporizing the pressurized water explosively. This is analogous to the bursting of a large overpressured bubble at the surface of a muddy lake. (c) An example of the velocity-time behavior of two kaolin suspensions showing that the velocity wanes after a peak value is reached. We mark the qualitative regimes that are associated with each window of velocity and which are explored in this study. Inset: still images from the high-speed videos showing a time evolution of the material ejected for two values of ϕ.

We loaded kaolin-water mixtures ($0 \leq \phi \leq 1$) into a 25 mm diameter, 60 mm height sample tube that was in turn loaded into a steel autoclave. The sample filled the tube volume. Above the kaolin-water mixture was a volume of gas approximately equal to the volume of the fluid. The autoclave was sealed by three to four aluminum foil layers and was heated by an external furnace to 120°C at a heating rate of 15°C min^{-1}, and temperature was monitored by a thermocouple at the base of the sample (Figure 2a). The application of heat resulted in gas pressurization above the sample. As the water in the sample reached the boiling curve for water, the pressure increased further until the boiling pressure of 2 bar (Figure 2b) resulting in a negligible volume reduction of water [*Montanaro et al.*, 2016]. Water and clay volume are conserved. Near-instantaneous rupture of the aluminum foil was triggered by externally rapidly increasing argon pressure in between two foil layers, causing rapid decompression of the sample down to ambient pressure. For the sample $\phi = 1$, a few droplets of water were added. Our *P-T* conditions were selected to represent a minimum condition that would be consistent with the observations of the microeruptions of White Island and bubble-burst events at the surface of the crater lake [*Jolly et al.*, 2016]. For the boiling of water in a fixed volume system such as this, see *Montanaro et al.* [2016]. We note that the difference in μ between 20°C at ambient pressure and 120°C pressurized to 2 bar is -1 order of magnitude. However, the difference in viscosity across the clay contents and shear rates investigated here is far greater, and so we conclude that the temperature effect is less than the suspension effect.

The rapid decompression event resulted in vigorous boiling of the water phase, nonlinear cooling (see Figure 2b for the pressure temperature path after the peak condition), and ejection of the suspension from the vent into the low-pressure tank above (Figure 2a; see section 3). The lowermost section of the low-pressure tank is backlit transparent acrylic, through which the ejection of the sample material could be recorded using a monochromatic high-speed Phantom V711 camera (Vision Research™) operating at 10,000 frames per second. The resultant videos were analyzed using ImageJ [*Abràmoff and Magalhães*, 2004], with which we used the MTrackJ plugin to track individual objects in time and space. For the largest particles, there is some uncertainty in the determination of particle velocity due to small rotational components of velocity. To minimize this, we tracked the motion of the central point of the particle rather than any particular edge pixel assuming that the particle did not itself deform during ejection. Another source of potential error arises from particle motion toward or away from the camera. We used a moderate focal depth (*f*4.0) which permitted us to determine when a particle moved out of focus in the plane of the camera, in which case we discarded data associated with this particle.

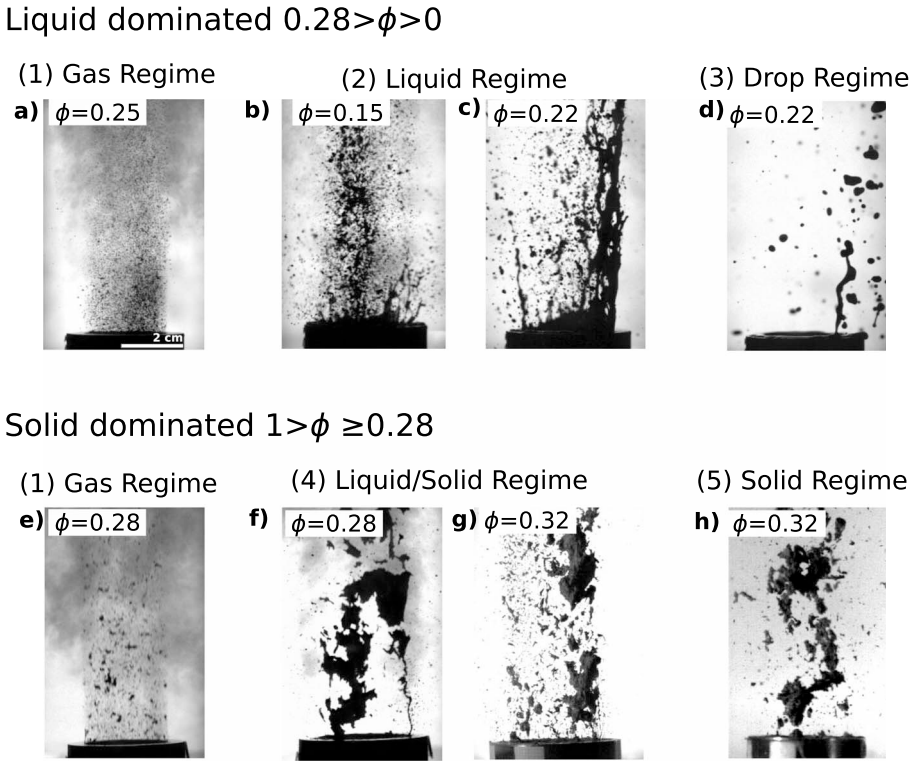

Figure 3. Schematic diagram of the regime observations found in this study for (a–d) $\phi < \phi_I$ and (e–h) $\phi > \phi_I$. Each regime is named and corresponds to the regime map given in Figure 4.

3. Results

With high-speed videography we observe ejection of the samples from the vent location to 15 cm height above the vent. Throughout the full range of ϕ (and at the *P-T* conditions analyzed in this study) the vigorous boiling of the sample produced either individual droplets, individual angular particles, elongate fluidal structures, or complex mixed behavior at the vent. The morphology of the ejecta evolved through time as the decompression-driven current velocity waned. For all ϕ, the first arrival at the vent was a condensing vapor phase (mixed argon water) in an overexpanded jet which quickly collapsed and was followed by the first sample material (see videos provided in the supporting information).

The velocity of the ejected sample material, averaged over the 3–5 cm above the vent, decays from a high initial value of ~50–70 m s^{-1} toward zero as ejection progressed from an initial time of decompression $t = 0$ to a maximum time $t = 0.18$ s. The maximum velocity at $t = 0$ was apparently dependent on ϕ. Qualitatively, at the vent, for low ϕ, the flow exhibited a short acceleration phase prior to reaching maximum velocity and then waning. For high ϕ, the flow was waning by the time ejecta reached the vent location (Figure 2c). In what follows we describe qualitatively the regimes of sample ejection behavior through time and space for different ϕ.

For all ϕ, the first regime observed was a jet phase (gas regime 1; Figure 3) in which collimated ejecta were dispersed in a water vapor and gas phase. The duration of this first regime was strongly dependent on ϕ. At high ϕ, the ejecta formed small angular particles, while at low ϕ, the ejecta formed small droplets. The approximate boundary between these end-members occurs at $0.25 < \phi < 0.28$ below which the sample is liquid dominated and above which the sample is solid dominated; definitions will be discussed later (Figures 3a and 3e).

Following the jet phase (gas regime 1), the liquid-dominated system ($\phi \leq 0.28$) and the solid-dominated system ($\phi \geq 0.28$) deviate in terms of bulk ejection behavior.

In the liquid-dominated system (for $\phi < 0.28$), the jet phase evolves to a liquid regime (regime 2; Figures 3b and 3c) in which fluidal structures appear at the vent. Following this, as the current wanes and the velocities

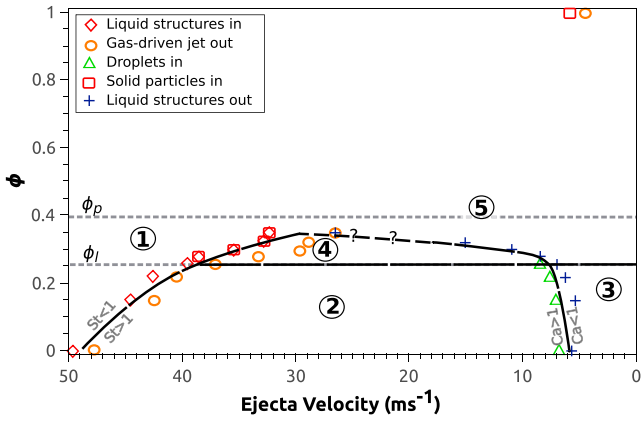

Figure 4. Regime diagram for the ejection behavior of clay suspensions from eruptions through muddy lakes. Observations from the high-speed videos used to constrain the beginning and end of ejection regimes. Here the red diamonds represent the first appearance of liquid (Figure 3b) or solid (Figure 3f) structures that are apparently uncoupled to the jet phase, while the orange circles represent the final frame in which a gas jet behavior could be identified (Figures 3a and 3e). The red squares and the green triangles represent the first appearance of solid particles (Figures 3g and 3h) or droplets (Figures 3c and 3d), respectively, while the blue crosses represent the final appearance of liquid structures. The regime boundaries are drawn by hand to guide the eye between these thresholds. We label the liquid limit as $\phi_l = 0.255$ and the apparent plastic limit $\phi_p = 0.395$ after *Franklin and Krizek* [1969], which agrees well with the transitional behavior between liquid-like and solid-like ejection.

go to 0, the ejecta transition to individual droplets (regime 3; Figure 3d). In the solid-dominated system (for $\phi \geq 0.28$), the jet phase evolves to the ejection of large (millimeter-sized to centimeter-sized) angular fragments with minor components of rare fluidal structures for $\phi \sim 0.28$ and the fluidal structures are entirely absent as $\phi \rightarrow 1$ (regime 4; Figures 3f and 3g). These rare fluidal structures are only seen at times soon after the jet phase and do not persist as the ejection progresses. The ejection of angular fragments with fluidal structures transitions toward the ejection of angular fragments without any fluidal structures as the current wanes (regime 5; Figure 3h).

4. A Regime Diagram for Mud Eruptions

We use the experimental observations (section 3) to define a regime diagram for ejection behavior of clay-rich suspensions. To do this, we define criteria characteristic of each regime. For example, the transition from regime 2 to regime 3 is defined as the first frame in the videos in which we observe individual droplet ejection (green triangles, Figure 4) and the last observation of elongated fluidal structures (blue crosses, Figure 4). Between the droplet-in and fluidal structures-out points, there is a mixed behavior, which results in uncertainty on the regime boundary. This same method of discrimination of regimes was applied to each transition marked in Figure 4, and the curves mark the approximate delineation between the closely spaced transitional behaviors. This results in a regime map of the ejection velocity at which we expect to observe particular behavior, for a given ϕ. For high ϕ, clay-rich suspensions are in the solid-dominated field, and we observe that such suspensions will evolve from a high-velocity jet regime to a regime in which solid particles are ejected at relatively low velocity. Contrastingly, we observe that for low ϕ, for which the system is liquid dominated, suspensions of clay will evolve from a high-velocity jet regime to a regime in which fluidal structures are ejected and finally to a regime in which individual droplets are ejected as the velocity wanes. Around $\phi = 0.28$, mixed behavior occurs in which the ejection of both fluidal and fragment structures is possible.

To understand the transition from one regime to another, we define dimensionless groups that characterize the behavior of particles and droplets in complex flows. These regime boundaries are conceptual physical limits and not strictly quantitative in the present case. First, the transition from a jet phase to the nonjet phases can be understood as the transition from a situation in which the ejected particles or droplets are coupled to the gas phase to a situation in which they are decoupled and relative velocities rise from zero. This can be characterized by a Stokes number *St*, which balances the timescale of flow with the timescale of particle motion opposing flow and is

$$St = \frac{u_g \lambda_p}{R}, \tag{1}$$

where λ_p is a particle motion timescale, u_g is the fluid velocity, and R is a characteristic particle size. For our case, λ_p is a timescale characteristic of settling under gravity. In our system we do not see the point where the continuous sample separates into individual fragments, droplets, or fluidal structures, which occurs below the point of observation. Nevertheless, at the point of observation, the ejecta have a velocity near

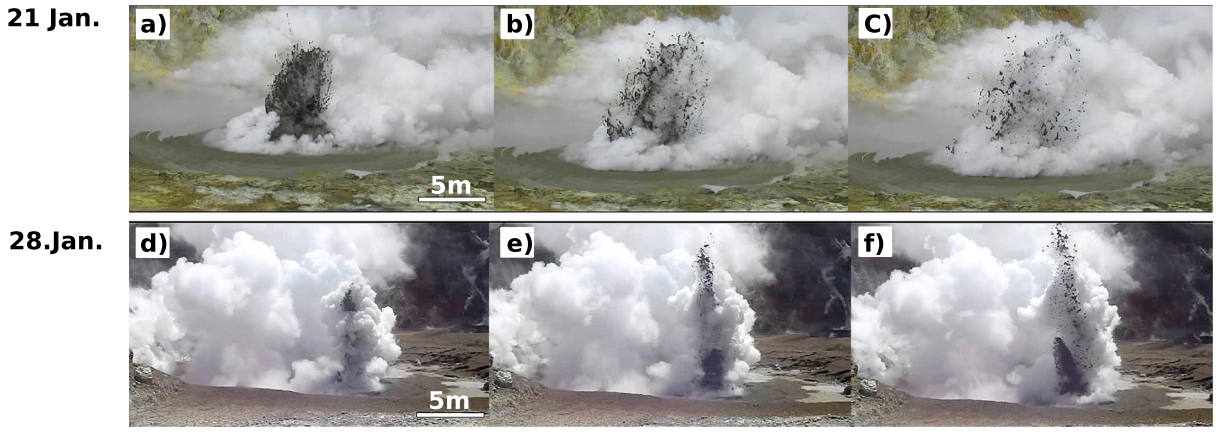

Figure 5. Still images from the 2013 eruptive episode through the muddy crater lake at White Island on (a–c) 21 January and (d–f) 28 January. Figures 5a–5c show a time evolution of an eruptive burst that is qualitatively liquid dominated, and Figures 5d–5f show a burst that is apparently solid dominated. The latter event has a mud heave associated with the late-time behavior, described in *Jolly et al.* [2016] and *Edwards et al.* [2017].

to the peak velocity. They are initially approximately coupled to the gas phase, evidenced by the rapid motion of the condensing water vapor in the jet, implying $St < 1$. This is consistent with a very low velocity of the particles with respect to the fluid. The end of the jet phase is then interpreted to be the point when the velocity of the gas phase wanes rapidly during expansion into the decompression tank so that $u_g \rightarrow 0$. As the gas velocity wanes, the relative velocity increases proportionally and *St* climbs above unity, at which point the ejecta become decoupled from the motion of the gas. Therefore, *St* is a measure of the regime boundary between regime 1 and the subsequent regimes of ejection.

In the liquid-dominated system ($\phi < 0.28$) the transition from liquid structures of fluidal elongate bridges (regime 2; Figure 4) to individual liquid droplets (regime 3; Figure 4) occurs when the relative velocity between the liquid phase and the ambient fluid phase falls to sufficiently low values that the surface tension at the liquid-gas interface dominates over shearing stresses. The capillary number *Ca* characterizes this competition and is

$$Ca = \frac{\eta R \dot{\gamma}}{\Gamma}, \tag{2}$$

where η is the dynamic viscosity of the clay-rich suspension (Figure 1), R is the characteristic size of the liquid droplet or fluidal bridge, Γ is the surface tension, and $\dot{\gamma}$ is the shear strain rate at the liquid-fluid interface. The shear strain rate is not easy to determine exactly, and the liquid viscosity is a nonlinear function of the shear strain rate (Figure 1). We suggest that this regime transition should conceptually occur when *Ca* is of order unity and the velocity at which this transition occurs is a weak increasing function of ϕ. This is consistent with observations that the dependence of η on ϕ is relatively small below $\phi = 0.3$ [*Chong et al.*, 1971]. This is possibly controlled by what is termed the *liquid limit* $\phi_l = 0.255$ in kaolin-water mixtures, which is when the mass fraction is $N = 0.47$ [*Franklin and Krizek*, 1969].

The transition from the liquid-dominated ($\phi < 0.28$) to the solid-dominated regime ($\phi \geq 0.28$) manifests itself as a transition from experiments that resulted in a final regime of liquid droplet morphology (regime 3) to experiments that resulted in solid-fragment morphology (regime 5). The occurrence of this transition at $\phi = 0.28$ is consistent with the liquid limit of $\phi_l = 0.255$ for kaolin suspensions at which the dependence of η on ϕ is discontinuous [*Franklin and Krizek*, 1969]. *Franklin and Krizek* [1969] additionally report the onset of plasticity in clay-rich suspensions occurring at $\phi = 0.395$. This window $0.255 \leq \phi \leq 0.395$ therefore represents the viscous-to-brittle transition in ejection behavior of particles from clay-rich substances in eruption.

5. Discussion

In Figure 5 we show still images from a video of mud eruptions at the White Island crater lake in 2013. These images demonstrate the two end-member scenarios discussed here: (1) the ejection of droplets and fluidal structures and (2) the ejection of discrete particles with apparent angularity. We can now interpret this as a

function of the local ϕ value relative to the liquid limit ϕ_l. The fact that several ϕ could be found in the same lake in the same eruptive episode lends support to the observations of *Edwards et al*. [2017] who invoked regular and rapid overturn and convection in such lakes, presumably mixing domains of variable clay content. The work of both *Edwards et al*. [2017] and *Jolly et al*. [2016] shows that the eruption mechanisms of these kind of ejection events is complex; we concur with these authors that the variability of ϕ locally in the lake fluid (the rheology) is a first-order parameter controlling whether an eruption will produce droplets or particles. We suggest that our experimental campaign yields the constraint necessary to make quantitative estimations of fine solid fraction from the observations of ejection velocity and approximate ejecta geometry. Additional factors that could account for changes in eruptive behavior include changes in lake temperature and polydispersivity of suspended solid particle sizes.

We propose that the liquid limit in clay suspensions represents a limiting water content above which the response of the material to a deformation is dominantly elastic and is controlled by frictional contact interactions between clay particles. Below this limit, the material behaves more like a conventional suspension of solid particles in a fluid. In this wet limit, the rheology is controlled by the volume fraction of clay particles (Figure 1). The viscous-to-brittle transition is therefore defined simply. However, at larger driving pressures than tested here (Figure 2) or than found at White Island's 2013 eruptive episode [*Jolly et al.*, 2016], we might expect higher ejection velocities [*Alatorre-Ibargüengoitia et al.*, 2010] and higher strain rates in which case the inertia of the ejection could result in local brittle-like behavior, especially at the concentrated end-member of high ϕ. This is a regime that would be a worthy frontier for future research. However, at most bubbling or exploding mud lakes, the overpressure driving eruption, determined by infrasound measurements, is typically low (as shown at White Island) [*Jolly et al*., 2016].

Other volcanic events that involve a release of overpressure and the resultant ejection of particles, however, involve larger overpressures and ejection velocities [*Bello et al*., 2012], which may involve a different criterion for the viscous-to-brittle transition [cf. *Gonnermann*, 2015]. Indeed, all separation events of liquid domains that occur by the propagation of fractures [*Dingwell and Webb*, 1989] involve a local brittleness, excepting, perhaps, separation by the approach to singularities [*Eggers*, 1993].

6. Concluding Remarks

We use targeted experimental decompressions of clay suspensions at temperatures appropriate for surficial volcanic crater lakes or mud pools to constrain the viscous-to-brittle transition. We find that this transition in bulk behavior is controlled by the water to clay volume ratio. At high water content, the suspension is a hydrodynamic fluid that can break into ejected droplets when decompressed. At low water content, the suspension is a frictionally controlled, dominantly elastic solid and breaks into angular fragments when decompressed. This explains the range of behavior found in the 2013 hydrothermal explosion events at White Island where the behavior is sometimes characterized by viscous bubble bursts and other times by more vigorous explosive events in a drier lake. We emphasize that the kaolin used in our study is an analogue for the suspension found, for instance, in White Island's crater lake. Further fine tuning of the regime diagram for the regime changes accounting for different suspension types might render this work applicable to lava lake or Strombolian bubble burst events. Our work may provide the constraint necessary to estimate solid content (e.g., clay) of a suspension from optical observations of eruptive style alone.

Acknowledgments
We are grateful for constructive comments from Gert Lube, one anonymous reviewer, and to Andrew Newman for editorial assistance. We acknowledge funding from the European Research Council (grant EVOKES; 247076). This work was partially funded by EQC grant 14/667 (microeruptions) from New Zealand Ministry of Business, Innovation and Employment (MBIE).

References

Abràmoff, M., and P. Magalhães (2004), Image processing with ImageJ, *Biophotonics*, *11*(7), 36–42.
Alatorre-Ibargüengoitia, M., B. Scheu, and D. Dingwell (2010), Energy consumption by magmatic fragmentation and pyroclast ejection during Vulcanian eruptions, *Earth Planet. Sci. Lett.*, *291*(1), 60–69.
Balmforth, N., A. Burbidge, and R. Craster (2000), Visco-plastic models of isothermal lava domes, *J. Fluid Mech.*, *403*, 37–65.
Bello, E. E. L. Del, and J. Taddeucci (2012), An analytical model for gas overpressure in slug-driven explosions: Insights into Strombolian volcanic eruptions, *J. Geophys. Res.*, *117,* B02206, doi:10.1029/2011JB008747.
Chong, J. S., E. B. Christiansen, and A. D. Baer (1971), Rheology of concentrated suspensions, *J. Appl. Polym. Sci.*, *15*(8), 2007–2021, doi:10.1002/app.1971.070150818.
Christenson, B., A. Reyes, R. Young, and A. Moebis (2010), Cyclic processes and factors leading to phreatic eruption events: Insights from the 25 September 2007 eruption through Ruapehu Crater Lake, New Zealand, *J. Volcanol. Geotherm. Res.*, *191*(1), 15–32.
Christenson, B., K. Németh, D. Rouwet, F. Tassi, J. Vandemeulebrouck, and J. C. Varekamp (2015), Volcanic lakes, in *Volcanic Lakes*, pp. 1–20, Springer, Berlin.
Coussot, P. (1995), Structural similarity and transition from Newtonian to non-Newtonian behavior for clay-water suspensions, *Phys. Rev. Lett.*, *74*(20), 3971–3974, doi:10.1103/PhysRevLett.74.3971.

Dingwell, D. B., and S. L. Webb (1989), Structural relaxation in silicate melts and non-Newtonian melt rheology in geologic processes, *Phys. Chem. Miner.*, *16*(5), 508–516.
Edwards, M., B. Kennedy, A. Jolly, and B. Scheu (2017), Evolution of a small hydrothermal eruption episode through a mud pool of varying depth and rheology, White Island, NZ, *Bull. Volcanol.*, *79*(2), 16–26.
Eggers, J. (1993), Universal pinching of 3D axisymmetric free-surface flow, *Phys. Rev. Lett.*, *71*(21), 3458.
Fischer, T., C. Ramírez, and R. Mora-Amador (2015), Temporal variations in fumarole gas chemistry at Poás volcano, Costa Rica, *J. Volcanol. Geotherm. Res.*, *294*, 56–70.
Fournier, N., F. Witham, M. Moreau-Fournier, and L. Bardou (2009), Boiling Lake of Dominica, West Indies: High-temperature volcanic crater lake dynamics, *J. Geophys. Res.*, *114*, B02203, doi:10.1029/2008JB005773.
Franklin, A., and R. Krizek (1969), Complex viscosity of a kaolin clay, *Clays Clay Miner.*, *17*, 101–110.
Gonnermann, H. M. (2015), Magma fragmentation, *Annu. Rev. Earth Planet. Sci.*, *43*, 431–458.
Huang, X., and M. Garcia (1998), A Herschel-Bulkley model for mud flow down a slope, *J. Fluid Mech.*, *374*, 305–333.
Hulme, G. (1974), The interpretation of lava flow morphology, *Geophys. J. Int.*, *39*(2), 361–383.
Jolly, A., B. M. Kennedy, M. Edwards, P. Jousset, and B. Scheu (2016), Infrasound tremor from bubble burst eruptions in the viscous shallow crater lake of White Island, New Zealand, and its implications for interpreting volcanic source, *J. Volcanol.*, *327*, 585–603.
Mader, H. M., E. W. Llewellin, and S. P. Mueller (2013), The rheology of two-phase magmas: A review and analysis, *J. Volcanol. Geotherm. Res.*, *257*, 135.
Maron, S., and P. Pierce (1956), Application of Ree-Eyring generalized flow theory to suspensions of spherical particles, *J. Colloid Sci.*, *11*(1), 80–95.
Montanaro, C., B. Scheu, K. Mayer, G. Orsi, R. Moretti, R. Isaia, and D. B. Dingwell (2016), Experimental investigations on the explosivity of steam-driven eruptions: A case study of Solfatara volcano (Campi Flegrei), *J. Geophys. Res. Solid Earth*, *121*, 7996–8014, doi:10.1002/2016JB013273.
Oppenheimer, C. (1997), Remote sensing of the colour and temperature of volcanic lakes, *Int. J. Remote Sens.*, *18*(1), 5–37.
Varekamp, J. (2015), The chemical composition and evolution of volcanic lakes, in *Volcanic Lakes*, pp. 93–123, Springer, Berlin.